ELSEVIER

Journal of Nuclear Materials 245 (1997) 60–65

journal of nuclear materials

The hydrogen inventory in plasma exposed graphite surfaces

M. Langhoff, B.M.U. Scherzer *

Max-Planck-Institut für Plasmaphysik, EURATOM Association, Boltzmannstrasse 2, D-85748 Garching, Germany

Received 24 July 1996; accepted 6 December 1996

Abstract

The trapping of hydrogen in graphite was investigated during exposure to an rf-discharge. The target placed in the wall of the rf-reactor was investigated in-situ by ion beam analysis. The hydrogen inventory was found to be twice as high as expected from ion beam implantation experiments in the similar energy range ≤ 200 eV. Also an enhanced ion induced desorption by the energetic analyzing beam was observed. This leads to the conclusion that a buildup of a hydrogen rich C:H-layer is formed by the simultaneous impact of thermal and energetic (≤ 200 eV) hydrogen. A model is presented which explains the formation of the C:H-layer by a stitching process of methyl radicals forming on the surface. Time resolved trapping measurements were performed to test for a transient uptake of hydrogen during plasma exposure. No such phenomenon could be detected below 600 K. Also the supposition that metallic impurities are responsible for a dynamic inventory at room temperature could be disproved.

1. Introduction

As graphite is a prime candidate for the first wall material of magnetically confined thermonuclear fusion plasma devices, the hydrogen inventory in and the release from carbon is of great importance for plasma density control and overall tritium inventory of a future fusion reactor.

Over the last 20 years a great effort has been made to understand the trapping of energetic hydrogen impinging on graphite and the release of the implanted hydrogen [1–4]. As a result, several models have been developed, providing a fairly good description of ion beam implantation experiments [5–8]. In common they are based upon the principle of the 'overflowing bathtub' [3], which holds for temperatures between room temperature and about 900 K; i.e., after a certain fluence of impinging hydrogen ions the graphite becomes saturated and for each ion implanted thereafter one hydrogen atom is released [9–19]. At room temperature the saturation occurs at a H/C-ratio of 0.4, but decreases with increasing temperature. Desorption of the trapped hydrogen is possible thermally at temperatures corresponding to trap energies of 2.4 eV to 3.6 eV or induced by ions. However, without heating or ion incidence none of the implanted hydrogen is released spontaneously. In these simple terms the recycling at graphite walls in a fusion reactor should be understood at least qualitatively, namely after a short pumping period the graphite should saturate and the impinging flux onto the wall should be instantaneously recycled as long as the wall temperature is kept constant. At saturation the recycling coefficient is one.

In fusion experiments, however, the observed phenomena point to a partially transient uptake of hydrogen during plasma exposure. The gas consumption necessary to maintain a discharge at a certain density increases with the area covered with graphite [20,21]. The global recycling coefficient, i.e., the recycling coefficient averaged over the total vessel wall, is less than one. Another clue to a dynamic hydrogen inventory at temperatures around 600 K and below is given by experiments where the plasma is moved between the limiter and the inner wall both cladded with graphite tiles. For this case the particle balance can be modelled with a delayed release of at least part of the hydrogen inventory at the inner wall. [22,23]. One striking argument is also the outgassing of vessel walls after the discharge on a time scale of seconds to hours [21].

* Corresponding author. Osterwaldstrasse 59, D-80805 Munich, Germany.

PII S0022-3115(96)00746-5

From this difference in spontaneous release after ion implantation and plasma exposure, respectively, the question arises whether the impact of a plasma on the graphite surface can be understood from ion beam implantation. Whereas typical experiments with ion beams deal only with monoenergetic hydrogen ions, the plasma–wall interaction involves molecular, atomic and ionic species with a broad energy range. Resulting synergistic effects have been observed and modeled for the chemical erosion of graphite [24–27]. The observation of the hydrogen retention in plasma experiments, however, suffers from the buildup of C:H-layers [28–30]. Therefore, conclusions from the gas consumption of the discharge to the transient pumping of graphite cannot be drawn. A second problem in the interpretation of quantitative measurements of the hydrogen inventory in plasma experiments is the poorly known energy distribution function of the impinging particles [31–34].

To check the validity of today's conception of hydrogen implanted in graphite during plasma–wall interaction the hydrogen inventory was observed in-situ during and after the exposure to an rf-plasma.

2. Experimental

The rf-reactor (Fig. 1) consists of a grounded plate and a cylindrical electrode enclosing a plasma volume of about 1 l. It is powered via a tuning matchbox by an rf-transmitter operated at 13.56 MHz with 60 W. The discharges were run in deuterium with a pressure of 10 Pa. The graphite target (Ringsdorff EK98) is placed in the grounded electrode.

A 2.6 MeV $^4He^+$-beam entering the chamber through an orifice system allows for in-situ ion beam analysis. At a scattering angle of 30° a surface barrier detector for elastic recoil detection analysis (ERDA) was mounted outside the reactor to determine hydrogen and deuterium inventories. The recoil atoms pass the reactor wall through an orifice

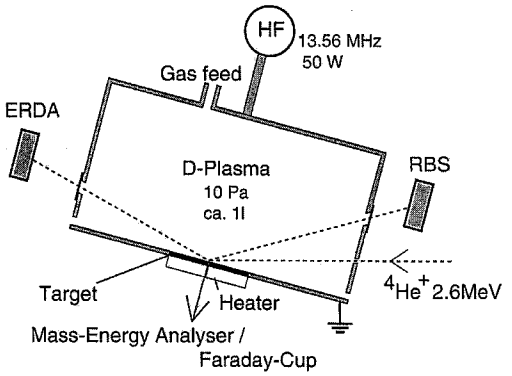

Fig. 1. The experimental setup. The complete apparatus is placed in a high vacuum vessel.

covered with a 5 μm thick stainless steel foil to hinder plasma ions and forward scattered ^4He – ions to reach the detector. A second detector (scattering angle 165°) was installed in the same way for simultaneous Rutherford backscattering (RBS) for monitoring impurities and measuring the analysing fluence (see below). To protect this detector from incident low energy plasma particles a 44 nm thick carbon foil was used. To achieve a high accuracy for the hydrogen and deuterium inventory a large solid angle was established for the ERDA detector, therefore resulting in a poor depth resolution.

The analyzing fluence for each data point was determined by the yield of a certain energy interval in the RBS spectra of carbon. The interval was chosen to correspond to a depth that could not be reached and therefore not be modified in any way by the plasma ions.

The energy distribution of ions incident from the plasma was measured with a mass–energy analyzer mounted behind the graphite target. A hole with 0.1 mm diameter in the target was used as the entrance orifice. An upper limit for the implanting ion energies can be given to be 220 eV corresponding to a range of deuterium in the carbon of 4.4×10^{20} atoms/m^2. The total ion flux was determined to 4×10^{18} ions/m^{2}s by a Faraday cup mounted temporarily behind the target instead of the mass–energy analyzer.

Because of the small orifices in the plasma reactor the pumping rate was very low. Consequently the discharge gas was mixed with hydrogen and oxygen impurities desorbed from the chamber walls by the plasma. Therefore, both the hydrogen and the deuterium inventory have to be taken into account and are summed up to one number in the following being denoted hydrogen inventory.

3. Results and discussion

After switching on the plasma the hydrogen inventory in the graphite increases in two steps (see Fig. 2). Initially a fast increase can be observed with a characteristic time of about 20 s. This is followed by a slow increase over about 700 s up to an inventory of $(8.8 \pm 0.8) \times 10^{20}$ atoms/m^2. Considering the low ion flux of 4×10^{18} ions/m^2 s one can conclude immediately that the ions alone cannot be responsible for the fast increase; a large flux of atomic hydrogen has to be involved. For comparison the behavior of the inventory is drawn in Fig. 2 expected from an implantation experiment with a monoenergetic ion beam of the highest energy of 220 eV and the same flux. It was calculated numerically following the local mixing model by Möller and Scherzer [7]. Apart from the initial increase corresponding to much more than 100% trapping of the incident ions another striking feature is the absolute value of hydrogen inventory that is about a factor two larger than expected from ion beam experiments.

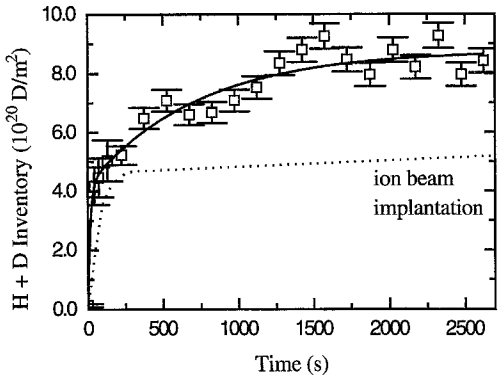

Fig. 2. Increase of the hydrogen inventory due to plasma exposure (data points). The dotted curve is to compare with ion beam implantation.

Assuming this high inventory to be responsible for a spontaneous release of hydrogen after implantation as observed in fusion machines, the hydrogen inventory was analyzed after switching off the plasma. In Fig. 3 the increase of the hydrogen inventory is shown up to a saturation level during plasma exposure (from 0 s to 300 s). After 300 s the discharge is switched off. No decrease in the hydrogen inventory is actually found (Fig. 3) in the time interval where no ion beam analysis was done (300–600 s). A decrease starts, however, immediately after starting the analyzing beam (at 600 s) as a result of ion induced desorption. In case of a spontaneous release the hydrogen inventory should have dropped in the time interval from 300 s to 600 s. No difference, however, was found between the two measurements in dependence of the fluence within an error limit of 5×10^{19} atoms/m^2. The experiment was repeated also at a target temperature of 600 K, which is the wall temperature in several fusion experiments. Thus, a dynamic hydrogen inventory could not be observed within the above mentioned error limit. Therefore the transient uptake of hydrogen in the first wall of fusion experiments cannot be explained by a genuine difference between plasma exposure and ion beam implantation.

One may speculate that impurities on the graphite tiles in fusion experiments are responsible for such a mobile hydrogen inventory [35,36]. Especially metals exhibit such a behavior under hydrogen bombardment [37]. Therefore a variety of metal impurities have been deposited onto the graphite target in our rf-plasma experiment. The impurities are produced by sputtering of the surrounding electrode by the plasma and redepositing on the target. Experiments were performed with a stainless steel electrode creating iron and chromium impurities and a second one coated with tungsten and molybdenum. In effect a topological graphite structure developed consisting of small cones (0.1 μm diameter and up to 5 μm long). This is well known from experiments with ion beams seeded with impurities [38,39] and has been reported previously [40]. Consequently the hydrogen inventory increases because of the increase of the surface area. Therefore, above experiments for testing on dynamic inventory could be performed with excellent accuracy. No spontaneous release could be observed in this case within an error limit of less than 3×10^{19} atoms/m^2. The earlier reported assumption that metallic impurities are responsible for a mobile hydrogen inventory at room temperature [36] was identified as an artifact of the underestimated ion induced desorption during analysis.

This ion induced desorption, however, with a cross section of $(1.6 \pm 0.4) \times 10^{-20}$ m^2 turned out to be higher than expected from ion beam implanted graphite. The cross section for the desorption of implanted hydrogen by He-ions in the MeV-range has been investigated by Roth et al. to be in the order of 10^{-22} m^2 [41]. Because of its dependence on the graphite structure and implantation energy the measurement was repeated for the fine grain graphite (Ringsdorff EK98) implanted at an energy of 300 eV. The result is a cross section of $(2.6 \pm 1.0) \times 10^{-21}$ m^2, which is still one magnitude lower than the desorption from the plasma exposed surface. A decrease with this cross section observed for ion beam implantation is also documented in Fig. 3.

With the increasing amount of impurities on the plasma exposed surface, however, the cross section decreases for this enhanced ion induced desorption and asymptotically approaches the above value for the ion beam implanted graphite.

It is generally established that ions in the MeV range are mainly stopped inelastically by the interaction with electrons. For the energy transfer to the electrons of a carbon atom it is found that it is higher if hydrogen is bound to carbon, compared to a free carbon atom [42,43]. The influence of the enhanced energy transfer to the ion

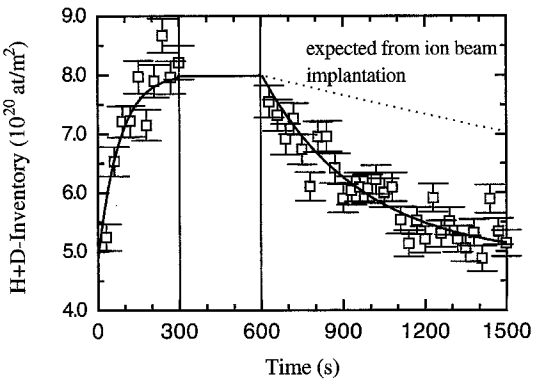

Fig. 3. The test for a transient uptake of hydrogen: Between 300 s and 600 s no hydrogen is lost. The decrease after 600 s is due to an enhanced ion induced desorption by the analysing beam. The dashed curve shows the ion induced desorption for ion beam implanted EK98 with 300 eV deuterium.

induced desorption of hydrogen has been confirmed for polymer-like C:H-films [43]. Therefore the assumption that a hydrogen rich C:H-layer is formed in the case of a plasma exposed surface explains the observed phenomena:

(i) The enhanced ion induced desorption, since it is due to electronic stopping, which is increased by chemical bonds.

(ii) The high hydrogen concentration, because of a polymer like film formation.

(iii) The fast initial increase, derived from the flux of atomic hydrogen necessary for the formation of the C:H-layer. This will be modelled in the following chapter.

The measurement with metallic impurities implies that they should hinder the formation of a C:H-layer. As the graphite surface is eroded effectively with a rate of about 0.1 nm/s the formation of a C:H-layer seems venturous, but the following model will show a possible way.

4. The model

To simplify the problem the bombarding hydrogen flux will be divided into an energetic part with energies of about 200 eV and a second one with thermal energies. Following the model of synergistic effects of simultaneous erosion by energetic ions and thermal hydrogen atoms of Haasz et al. [24], thermal atoms are forming CH_3-radicals desorbing from the very surface whereas the ions are implanted 'deep' into the graphite. Therefore the plasma exposed surface will be sectioned into three layers (see Fig. 4): the very surface, where methyl radicals are formed, a second layer that will be the forming C:H-layer and the implantation zone which is defined by the maximum range of the energetic hydrogen.

The development of C:H-layers in general is believed to be due to the ion induced stitching process [44], i.e., transforming adsorbed CH_3-radicals from the plasma into an interconnected C:H-network. Whereas usually the origin for the methyl radicals is the hydrocarbon plasma in the case of a hydrogen plasma eroding the surface methyl radicals are formed at chemically active sites on the surface by the thermal hydrogen. It is assumed that only part of them desorb, whereas the rest is built into the C:H-layer by stitching of the energetic hydrogen ions. The mathematical formalism will be presented in Appendix A.

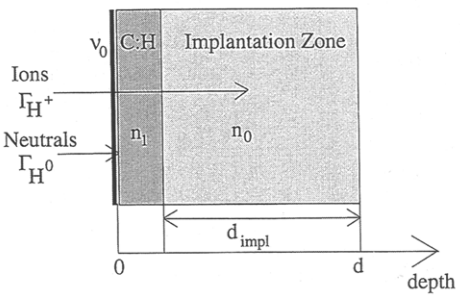

Fig. 4. The model of the C:H-layer buildup: At the very surface, methyl radicals are incorporated into the C:H-layer by stitching due to the energetic plasma ions.

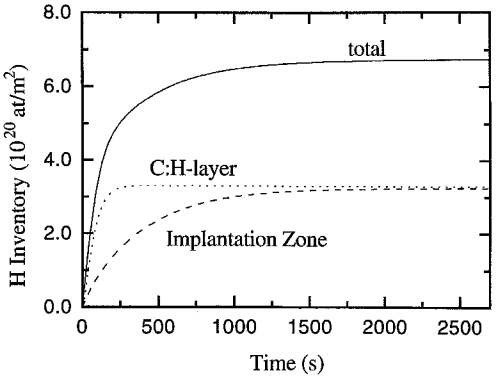

Fig. 5. A model calculation of the hydrogen inventory due to the buildup of the C:H-layer under plasma exposure.

As the model is based on a set of parameters that are not very well known, it can only be expected to give a qualitative description of the process. In Fig. 5 is shown a simulation of the hydrogen inventory in the graphite target during the plasma exposure in the rf-discharge. The unknown thermal hydrogen flux is estimated by the assumption of 100% trapping at the beginning plasma exposure. One key parameter totally unknown is the residence time of CH_3-radicals on the surface before desorbing. It was fitted such that the CH_3-emission is compatible with measurements of Haasz et al. [24]. The H/C-ratio in the C:H-layer was arbitrarily assumed to reach 1.5, which is possible for a polymerlike film [44]. All other parameters are taken as reported in the literature and discussed in detail in Appendix A.

As one can see in Fig. 5, the formation of a C:H-layer can actually be explained by this model. The hydrogen inventory in the C:H-layer reaches values that are comparable to the one in the implantation zone. Also the two time scales, the fast initial increase of the inventory and the slow one afterwards, can be assigned to the fast buildup of the C:H-layer and the slow implantation due to the ion flux. For graphite surfaces with metallic impurities it can be assumed that a metal covered carbon atom cannot be hydrated to a CH_3-group to be desorbed or built into the C:H-layer. Therefore the hydrogen ratio should decrease, which is seen in the beginning. But after a short time the effect is superimposed by a vast increase due to the formation of the cone structure. Nevertheless, the decrease of the enhanced cross section for ion induced desorption indicates that the C:H-layer vanishes with higher impurity concentration.

The formation of the C:H-layer is crucially dependent on the two fluxes of different energies. Therefore, this phenomenon should not be observed necessarily on any

surface reached by energetic and thermal hydrogen. On the other hand, the hydrogen inventory becomes flux dependent, which could explain the transient uptake of hydrogen in the wall of fusion experiments during the discharge: Assuming the buildup of such a C:H-layer at some part of the vessel surface, this could lead to an enhanced desorption process due to only a low ion flux, e.g., charge exchange neutrals, if the plasma is changed such that the formation of the C:H-layer stops. The slow outgassing after the discharge, however, can only be explained by the assumption of the development of an unstable C:H-layer that releases hydrogen spontaneously. One may speculate that this could happen due to the unusually high fluxes occurring in fusion experiments.

5. Conclusions

Graphite exposed to an rf-discharge has been found to exhibit a higher inventory and also an enhanced cross section for ion induced desorption. This behavior can be understood by the assumption that a hydrogen rich polymer like C:H-layer forms on the surface. A model has been presented that explains the possibility of the formation due to ion induced stitching of desorbing CH_3-groups created by the bombardment of hydrogen with low energies. The inventory of this C:H-layer is dependent on the hydrogen flux. A transient uptake of hydrogen, however, has not been found.

Appendix A

The three layers, namely surface, C:H-layer and implantation zone, are modelled by the following differential equations using the following symbols:

- Θ surface coverage with CH_3-groups
- ν_0 number of surface sites available for the formation of CH_3-groups, with respect to the surface roughness assumed as 5×10^{19} atoms/m^2
- τ residence time of CH_3-radicals on the surface before desorption takes place
- Γ_{H^0} flux density of thermal hydrogen
- Γ_{H^+} flux density of energetic hydrogen
- σ_{st} stitching coefficient, 10^{-19} m^2, taken from Ref. [45]
- n_0 areal density of hydrogen in the implantation zone
- n_1 areal density of hydrogen in the C:H-layer
- c_{max} maximum concentration of hydrogen in the implantation zone, i.e., 0.4
- c the actual concentration in the implantation zone, equals to n_0/d_{impl}
- f fraction of the hydrogen flux deposited into the C:H-layer, approximately fraction of the depth of the two zones
- Y_{CH_4} chemical erosion yield, i.e., 0.01, from Ref. [46]
- r introduced hydrogen per CH_3-radical, which is taken as a high C/H-ratio of 1.5 observable in C:H-layers
- $\sigma_{C:H}$ cross section for ion induced desorption of the hydrogen ions, see below
- d maximum depth of hydrogen as carbon areal density, i.e., 10^{21} C/m^2
- d_{impl} thickness of the implantation zone as carbon areal density.

The first equation describes the surface coverage Θ with CH_3-radicals:

$$\partial_t \Theta = (1-\Theta)\frac{1}{3}\frac{\Gamma_{H^0}}{\nu_0} - \frac{\Theta}{\tau} - \Theta\Gamma_{H^+}\sigma_{st}. \tag{A.1}$$

The first term denotes the hydration process of surface sites by the thermal hydrogen. The surface coverage is then reduced either by desorption (second term) or by the stitching process (last term).

The following equation balances the hydrogen areal density n_1 in the C:H-layer:

$$\partial_t n_1 = r\Theta\Gamma_{H^+}\sigma_{st}\nu_0 - 4f\Gamma_{H^+}Y_{CH_4} - \sigma_{C:H}f\Gamma_{H^+}n_1 \tag{2}$$

The first term introduces a part r of the stitched CH_3-radical to the hydrogen inventory in the C:H-layer. A second term accounts for the erosion in a simple way describing a fraction f of the incident ion flux to form desorbing CH_4 molecules. The last term accounts for the loss by desorption of hydrogen due to the energetic hydrogen.

The third equation is the 'overflowing Bathtub'-concept valid for the implantation zone.

$$\partial_t n_0 = \left(1 - \frac{c}{c_{max}}\right)(1-f)\Gamma_{H^+} - 4\frac{c}{c_{max}}Y_{CH_4}(1-f)\Gamma_{H^+}. \tag{3}$$

The first term implants hydrogen as long as the concentration c is lower than c_{max}. Only the part $(1-f)$ of the energetic flux reaches the implantation zone. To account for the correct erosion yield the second term gives an approximation for the chemical sputtering in the implantation zone. Therefore the yield Y_{CH_4} measured for saturated graphite is reduced by the ratio of actual to maximum hydrogen concentration.

For the description of the depth of the two layers the last equation is necessary, which is for the carbon areal density of the implantation zone:

$$\partial_t d_{impl} = \frac{d - d_{impl}}{n_1}\sigma_{C:H}f\Gamma_{H^+}n_1 - \Theta\nu_0\sigma_{st}\Gamma_{H^+} + Y_{CH_4}f\Gamma_{H^+}. \tag{4}$$

If all hydrogen atoms bound to a carbon atom in the C:H-layer are desorbed, then this carbon atom can be

counted to the implantation zone (first term). The other two terms account for the gain or the loss of carbon atoms in the C:H-layer, which results in a shorter or larger range, respectively. This variation in the range affects only the implantation zone.

To obtain the hydrogen inventory as plotted in Fig. 5 the differential equations were integrated numerically with the Runge–Kutta method.

References

[1] S.K. Erents, in: Applications of Ion Beams to Materials, 1975, The Conference Series No. 28 (Institute of Physics, London, Bristol, 1976) p. 318.
[2] W. Möller and J. Roth, in: Physics of Plasma–Wall Interaction in Controlled Fusion, eds. D.E. Post and R. Behrisch (Plenum, New York, 1986) p. 439.
[3] K.L. Wilson and W.L. Hsu, J. Nucl. Mater. 145–147 (1987) 121.
[4] W. Möller, J. Nucl. Mater. 162–164 (1989) 138.
[5] B.L. Doyle, W.R. Wampler, D.K. Brice and S.T. Picraux, J. Nucl. Mater. 93&94 (1980) 551.
[6] S.K. Erents and E.S. Hotston, Nucl. Instrum. Meth. 170 (1980) 449.
[7] W. Möller and B.M.U. Scherzer, J. Appl. Phys. 64 (1988) 4860.
[8] A.A. Haasz, P. Franzen, J.W. Davis, S. Chiu and C.S. Pitcher, J. Appl. Phys. 77 (1995) 66.
[9] B.M.U. Scherzer, R. Behrisch, W. Eckstein, U. Littmark, J. Roth and M.K. Sinha, J. Nucl. Mater. 63 (1976) 100.
[10] G. Staudenmaier, J. Roth, R. Behrisch, J. Bohdansky, W. Eckstein, P. Staib and S. Matteson, J. Nucl. Mater. 84 (1979) 149.
[11] S.K. Erents, Nucl. Instrum. Meth. 170 (1980) 455.
[12] B.L. Doyle, W.R. Wampler and D.K. Brice, J. Nucl. Mater. 103&104 (1981) 513.
[13] W.R. Wampler, S.T. Picraux, S.A. Cohen, H.F. Dylla, S.M. Rossnagel and G.M. McCracken, J. Nucl. Mater. 102 (1981) 298.
[14] W.R. Wampler, D.K. Brice and C.W. Magee, J. Nucl. Mater. 102 (1981) 304.
[15] K. Sone and G.M. McCracken, J. Nucl. Mater. 111&112 (1982) 606.
[16] M. Braun and B. Emmoth, J. Nucl. Mater. 128&129 (1984) 657.
[17] B.M.U. Scherzer, J. Nucl. Mater. 168 (1989) 121.
[18] J.W. Davis, A.A. Haasz and D.S. Walsh, J. Nucl. Mater. 176&177 (1990) 992.
[19] A.A. Haasz and J.W. Davis, J. Nucl. Mater. 209 (1994) 155.
[20] H.F. Dylla and the TFTR team, J. Nucl. Mater. 145–147 (1987) 48.
[21] J. Ehrenberg, J. Nucl. Mater. 162–164 (1989) 63.
[22] J. Ehrenberg and P.J. Harbour, Nucl. Fusion 31 (1991) 287.
[23] C. Grisolia, P. Ghendrih, B. Pégourié and A. Grosman, J. Nucl. Mater. 196–198 (1992) 281.
[24] A.A. Haasz and J.W. Davis, J. Chem. Phys. 85 (1986) 3293.
[25] A.A. Haasz, J.W. Davis, O. Auciello, P.C. Stangeby, E. Vietzke, K. Flaskamp and V. Philipps, J. Nucl. Mater. 145–147 (1987) 412.
[26] J.W. Davis, A.A. Haasz and P.C. Stangeby, J. Nucl. Mater. 155–157 (1988) 234.
[27] E. Vietzke and V. Philipps, Fusion Technol. 15 (1989) 108.
[28] W.L. Hsu and R.A. Causey, J. Vac. Sci. Technol. A5 (1987) 2768.
[29] K. Akaishi, M. Asano, Y. Kobota and A. Miyahara, J. Vac. Sci. Technol. A9 (1991) 2747.
[30] M. Rubel, B. Emmoth, H.B. Ker, P. Wienhold, V. Dunaev and V. Sukholinov, J. Nucl. Mater. 196–198 (1992) 285.
[31] R.A. Causey and K.L. Wilson, J. Nucl. Mater. 138 (1986) 57.
[32] R.A. Causey, M.I. Baskes and K.L. Wilson, J. Vac. Sci. Technol. A4 (1986) 1189.
[33] Y. Hirooka, W.K. Leung, R.W. Conn, D.M. Goebel, B. LaBombard, R. Nygren and K.L. Wilson, J. Vac. Sci. Technol. A6 (1988) 2965.
[34] Y. Hirooka, R.W. Conn, D.M. Goebel, B. LaBombard, R. Lehmer, W.K. Leung, R.E. Nygren and Y. Ra, J. Nucl. Mater. 162–164 (1989) 1004.
[35] C. Jandl, W. Möller and B.M.U. Scherzer, in: Proc. 18th European Conf. Controlled Fusion and Plasma Physics, Europhysics Conference Abstracts, Vol. 15C, eds. P. Bachmann and D.C. Robinson (1991) p. III/245.
[36] C. Jandl, PhD thesis, TU München (1993).
[37] W. Möller, Nucl. Instrum. Meth. 209&210 (1983) 773.
[38] G.K. Wehner and D.J. Hajicek, J. Appl. Phys. 42 (1971) 1145.
[39] W. Hauffe, in: Sputtering by Particle Bombardment III, Topics in Applied Physics, eds. R. Behrisch and K. Wittmaack, Vol. 64 (Springer, Berlin, 1991) p. 305.
[40] M. Langhoff and B.M.U. Scherzer, in: Proc. 21st Eur. Conf. Controlled Fusion and Plasma Physics, Europhysics Conference Abstracts, eds. E. Joffrin, P. Platz and P.E. Stott, Vol. 18B (1994) p. II/782.
[41] J. Roth, B.M.U. Scherzer, R.S. Blewer, D.K. Brice, S.T. Picraux and W.R. Wampler, J. Nucl. Mater. 93&94 (1980) 601.
[42] J.R. Sabin and J. Oddershede, Nucl. Instrum. Meth. B27 (1987) 280.
[43] D. Boutard, B.M.U. Scherzer and W. Möller, J. Appl. Phys. 65 (1989) 3833.
[44] W. Möller, Appl. Phys. A56 (1993) 527.
[45] W. Möller, T. Pfeiffer and M. Schluckebier, Nucl. Instrum. Meth. 182&183 (1981) 297.
[46] J. Roth and J. Bohdansky, Nucl. Instrum. Meth. B23 (1987) 549.